Computers and Structures 320 (2026) 108033

Contents lists available at ScienceDirect

Computers and Structures

journal homepage: www.elsevier.com/locate/compstruc

Flexoelectricity effects on smart piezoelectric nanoplates using an isogeometric analysis-based Chebyshev shear deformation theory

P.T. Hung [a], H. Nguyen-Xuan [b], M. Abdel-Wahab [c,d,e], Chien H. Thai [f,g], P. Phung-Van [h,*]

[a] Faculty of Civil Engineering, Ho Chi Minh City University of Technology and Education (HCMUTE), Ho Chi Minh City, Viet Nam
[b] CIRTECH Institute, HUTECH University, Ho Chi Minh City, Viet Nam
[c] Soete Laboratory, Department of Electrical Energy, Metals, Mechanical Constructions and Systems, Faculty of Engineering and Architecture, Ghent University, 9000 Ghent, Belgium
[d] College of Engineering, Yuan Ze University, Taoyuan City, Taiwan
[e] Parallel and Distributed Systems Laboratory, Jožef Stefan Institute, Jamova cesta 39, SI-1000 Ljubljana, Slovenia
[f] Mechanics of Advanced Materials and Structures, Institute for Advanced Study in Technology, Ton Duc Thang University, Ho Chi Minh City, Viet Nam
[g] Faculty of Civil Engineering, Ton Duc Thang University, Ho Chi Minh City, Viet Nam
[h] Faculty of Civil Engineering, HUTECH University, Ho Chi Minh City, Viet Nam

A R T I C L E I N F O

Keywords:
Piezoelectric nanoplates
Flexoelectric effect
Size-dependent analysis
Isogeometric analysis (IGA)
Chebyshev shear deformation theory

A B S T R A C T

This study conducts a comprehensive investigation into free vibration and static behaviors of smart piezoelectric nanoplates, incorporating electromechanical coupling phenomena, particularly the flexoelectric effect. The flexoelectric effect, which characterizes the interaction between electric polarization and strain gradient, is considered by capturing size-dependent properties at the nanoscale. To enhance modeling accuracy, the third-order Chebyshev shear deformation theory is employed, naturally fulfilling the zero-shear stress conditions on the top and bottom surfaces of the plate without requiring supplementary constraints. For the computation of nanoplate displacement and natural frequency, isogeometric analysis is utilized to discretize the problem domain, offering superior geometric representation and computational efficiency. The present study systematically investigates the effects of flexoelectricity boundary conditions and material properties on structural behaviors of smart piezoelectric nanoplates. Numerical results demonstrate that the flexoelectric effect significantly enhances the stiffness and natural frequency of piezoelectric nanoplates, particularly for thinner structures. As thickness increases, this influence diminishes and the results converge toward classical predictions. The findings provide valuable insights for the design of nanoscale piezoelectric and flexoelectric devices in smart structural applications.

1. Introduction

Piezoelectric nanoplates considering flexoelectric effects combine the direct piezoelectric response with strain gradient-induced polarization, enabling enhanced electromechanical performance at the nanoscale. The flexoelectric effect, significant in nanoscale systems, introduces size-dependent behaviors crucial for designing advanced sensors, generators [1], actuators [2] and energy-harvesting devices. It should be emphasized that while the piezoelectric effect occurs only in non-centrosymmetric crystals, the flexoelectric effect is universal and can exist in all dielectric materials, thus broadening its applicability in nanoscale electromechanics. Recent theoretical developments on constitutive matrices of crystalline solids have clarified the coupling mechanisms between classical effects (elasticity, piezoelectricity, dielectricity) and higher-order effects such as couple stress and curvature-based flexoelectricity [3,4], providing a more general framework for analyzing these phenomena. In addition, studies on metamaterials based on couple stress theory have revealed unique mechanical couplings, such as axial force-torsion-warping interactions in materials with D_2 symmetry, which cannot occur in conventional continua [5]. These findings enrich the theoretical basis for understanding complex coupling behaviors at the micro- and nanoscale. Given these advances, accurate theoretical modeling of electromechanical coupling effects is essential to predict and optimize the performance of nanoscale structures. Accordingly, numerous studies have been devoted to investigating the electromechanical characteristics of smart nanostructures. For example, Yan

* Corresponding author at: Faculty of Civil Engineering, HUTECH University, Ho Chi Minh City, Viet Nam.
E-mail addresses: hungpht@hcmute.edu.vn (P.T. Hung), thaihoangchien@tdtu.edu.vn (C.H. Thai), pv.phuc86@hutech.edu.vn (P. Phung-Van).

https://doi.org/10.1016/j.compstruc.2025.108033
Received 3 September 2025; Accepted 6 November 2025
Available online 20 November 2025
0045-7949/

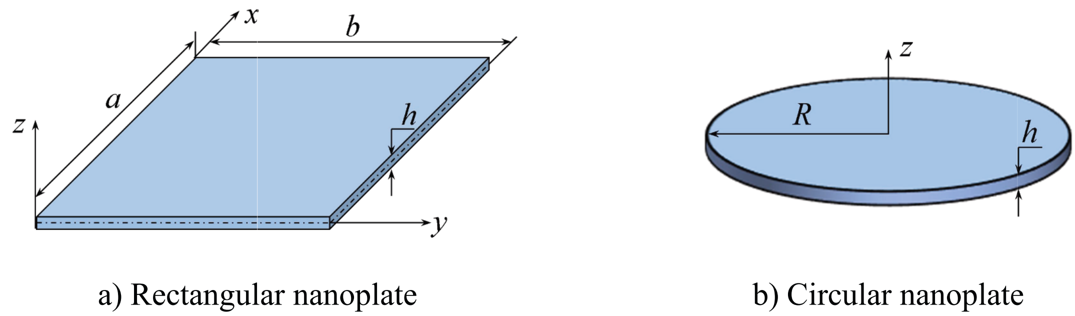

Fig. 1. Geometrical configurations of the flexoelectric piezoelectric nanoplates: (a) rectangular nanoplate, (b) circular nanoplate.

and Jiang employed an analytical method to examine buckling and free vibration of smart nanoplates with the surface effect [6] and static analysis of the flexoelectric nanobeams [7]. Qu et al. [8] developed a continuum theory for flexoelectric semiconductors based on finite deformation and strain-gradient mechanics. Vibration response of the flexoelectric piezoelectric nanoplate using Kirchhoff plate theory (KPT) and the analytical method was investigated by Zhang et al. [9]. Yue et al. [10] developed Timoshenko micro-beams for piezoelectric materials, incorporating flexoelectricity, surface effects and shear strain gradients. The findings highlighted the substantial role of flexoelectricity and surface effects in deformation and natural frequency variations. Moreover, the static behavior of cantilevered nanoplates using the KPT and extended flexoelectric theory was studied by Wang et al. [11]. The results showed that the flexoelectric effect becomes more pronounced in thinner plates and is sensitive to variations in boundary conditions, geometric aspect ratios and applied loads. Ebrahimi et al. [12–14] examined free vibration and buckling analyses of the smart nanoplates. The analysis incorporated surface and flexoelectric effects based on nonlocal elasticity theory and is carried out using an analytical method. Chu et al. [15] examined flexoelectric nanobeams based on a modified strain gradient theory (MSGT). The findings showed that the flexoelectric significantly influenced the electromechanical response of the smart nanobeam. Von Karman nonlinear analysis of smart nanoplates featuring a functionally graded (FG) porous core was studied by Zheng et al. [16]. Moreover, Amir et al. [17] carried out the free vibration analysis of flexoelectric plates supported on a Pasternak foundation. Results showed that increasing the thickness of the flexoelectric face sheets lowered the vibration frequency. Arani et al. [18] examined the role of flexoelectricity and surface effects on nanoplate vibrations, finding a significant rise in natural frequencies using FSDT and nonlocal elasticity theory combined with the differential quadrature method (DQM). Dhaba et al. [19] analyzed the static bending of anisotropic dielectric nanoplates under uniform loading using KPT and simplified strain gradient theory, revealing that the flexoelectric effect is more pronounced at the nanoscale and near the surface. Malikan and Eremeyev [20] found the analytical dynamic of the flexoelectric viscoelastic nanobeams based on nonlocal strain gradient theory (NSGT). Wang et al. [21] examined the free vibration of the piezoelectric nanoplate under the effect of flexoelectricity according to the KPT and analytical method. Yu et al. [22] investigated FG piezoelectric nanobeams and found that flexoelectricity influenced higher-order modes, while the gradient index affected the frequency and stiffness. According to the strain gradient theory DQM, Zhao et al. [23] explored the dynamic and static behaviors of the flexoelectric Euler-Bernoulli nanobeams. Xu et al. [24] explored the analytical size-dependent flexoelectric effect on piezoelectric circular nanoplates using KPT. Results revealed that flexoelectricity had a stronger impact on electrostatic responses than piezoelectricity at the nanoscale. Besides, bilayer flexoelectric circular nanoplates considering surface stresses were performed by Zhou et al. [25]. Liu et al. [26] studied electromechanical analysis of FG piezoelectric nanobeams with exponentially varying material properties. Xu et al. [27] examined the vibration of flexoelectric nanoplates using the KPT and Navier method. Nguyen et al. [28] studied buckling and static bending of FG nanoplates reinforced by graphene platelets (GPLs) using analytical solutions based on NSGT and surface elasticity theory. Vibrational behavior of the FG porous sandwich nanoplate with piezoelectric layers under hydro and thermal loadings was examined by Jearsiripongkul et al. [29] by using the NSGT. Zhang et al. [30] examined static, free vibration and buckling analyses of smart semiconductor nanoplates, employing analytical solutions and modified couple stress theory (MCST). In addition, Naskar et al. [31] presented the scale-dependent analysis of the piezoelectric functionally graded nanoplates incorporating graphene reinforcement based on the MCST and semi-analytical method.

The higher-order shear deformation theory (HSDT) offers a more accurate analysis of plate behavior compared to classical plate theory, which assumes negligible shear deformation. The HSDT with higher-order terms in the displacement field accurately accounts for shear deformation effects, making it particularly suitable for moderately thick plates where these effects are significant. Unlike the Mindlin–Medick theory and FSDT [32–34], which assume a constant shear strain distribution across the thickness and require the use of shear correction factors, HSDT eliminates this limitation by naturally capturing the parabolic variation of shear stresses without additional assumptions. Various HSDT models have been developed to accurately describe stress and strain distributions through the plate thickness. Examples include third-order shear deformation theory (TSDT) [35], exponential shear deformation theory (ESDT) [36], Quasi-3D theory [37], refined Quasi-3D theory [38], zigzag theory [39], and refined plate theory (RPT) [40], etc. However, HSDT formulations require C^1-continuity, a requirement that standard FEM cannot fulfill. To address this challenge, isogeometric analysis (IGA) with Non-Uniform Rational B-Splines (NURBS) basic functions is utilized to construct plate formulations compatible with HSDT. IGA, introduced by Hughes et al. in 2005 [41], combines finite element analysis (FEA) with computer-aided design (CAD) using NURBS for both geometry representation and simulation. While traditional methods have addressed piezoelectricity, they often overlook the coupling between strain gradients and polarization, which is crucial at the nanoscale. IGA offers enhanced accuracy and efficiency for complex geometries but has yet to be applied to piezoelectric nanoplates with flexoelectric effects. Future research could integrate IGA with flexoelectric theory to better capture size-dependent behaviors and improve the design of nanoscale devices like sensors and energy harvesters. In related work, Phung-Van et al. developed an effective model using the HSDT and IGA to perform the nonlinear transient behavior of FG piezoelectric plates [42] and the static, vibration and dynamic control of piezoelectric composite plates [43]. Ma et al. [44] used TSDT and IGA to present the static analysis of bi-directional FG plates with piezoelectric faces under initial electric potential. Whereas, Hasim and Kefal [45] studied bending analysis of smart laminated composite plates using IGA layer-wise element. Nguyen et al. [46] investigated electro-mechanical vibration analysis of FG piezoelectric porous microplates using HSDT, MSGT and IGA. In this article, IGA free

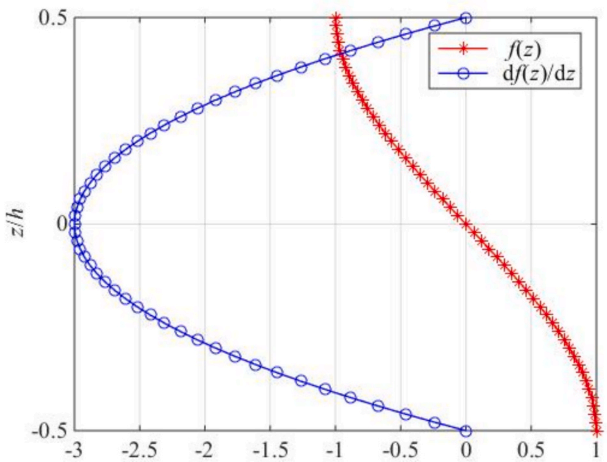

Fig. 2. Variation of the shear function f(z) and its derivative $\frac{df(z)}{dz}$ through the plate thickness.

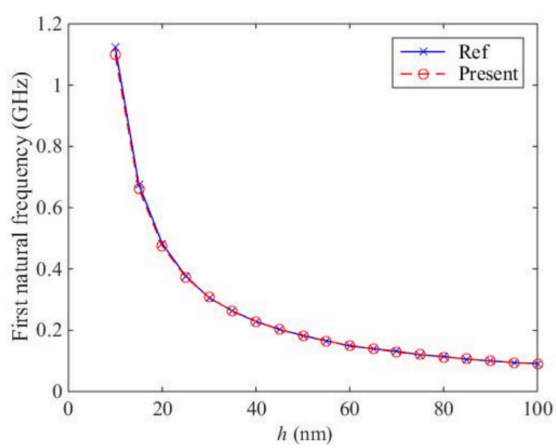

Fig. 3. The first natural frequency of the SSSS rectangular flexoelectric nanoplate ($a/h = 50$).

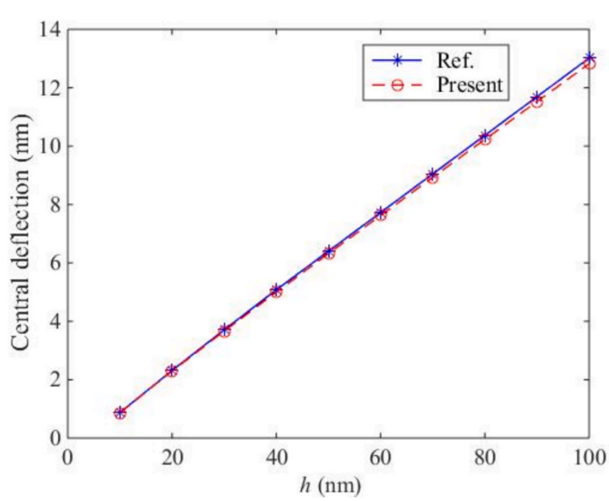

Fig. 4. The central deflection of the SSSS rectangular flexoelectric nanoplate ($a/h = 50$).

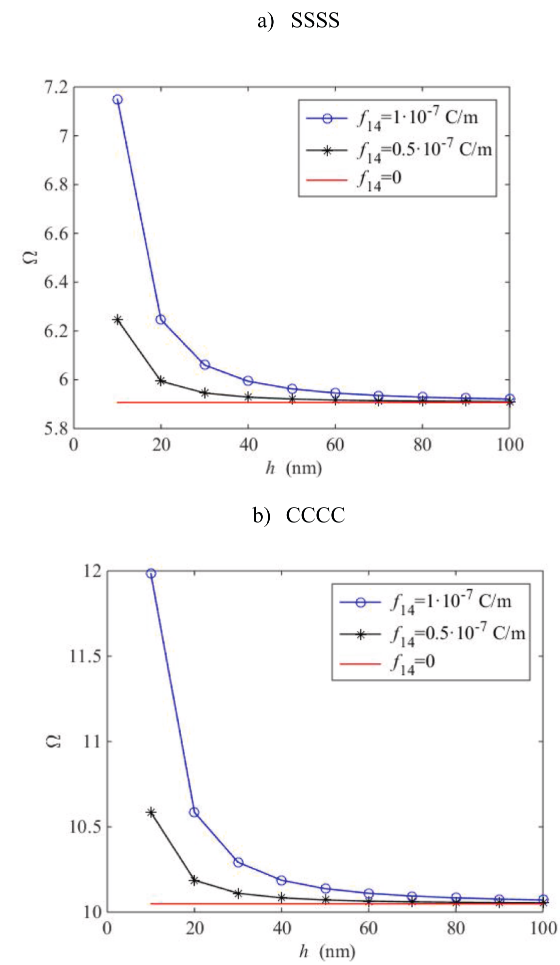

Fig. 5. The first dimensionless natural frequency of the flexoelectric square nanoplate ($a/h = 10$).

vibration and bending of the smart piezoelectric nanoplates considering the flexoelectric effect are studied for the first time. To improve modeling accuracy, the proposed third-order Chebyshev shear deformation theory (TCSDT), which naturally fulfills the condition of zero shear stress at the upper and lower surfaces of the plate, eliminating the need for extra constraints, is presented to describe the displacement of the flexoelectric piezoelectric nanoplates. NURBS functions are used to approximate the displacement fields of the nanoplate. The impact of flexoelectricity, material properties, and boundary conditions on the static deformation and natural frequencies of piezoelectric nanoplates is examined and discussed.

2. The fundamental formulations

2.1. The third-order Chebyshev shear deformation theory

In this investigation, TCSDT is utilized [47,48]. The displacements of smart piezoelectric nanoplates, as shown in Fig. 1, are expressed as follows

$$\widehat{\mathbf{u}} = \mathbf{u}_1 + z\,\mathbf{u}_2 + f(z)\mathbf{u}_3 \tag{1}$$

where

$$\widehat{\mathbf{u}} = \begin{Bmatrix} \widehat{u} \\ \widehat{v} \\ \widehat{w} \end{Bmatrix};\ \mathbf{u}_1 = \begin{Bmatrix} u \\ v \\ w \end{Bmatrix};\ \mathbf{u}_2 = \begin{Bmatrix} -w_{,x} \\ -w_{,y} \\ 0 \end{Bmatrix};\ \mathbf{u}_3 = \begin{Bmatrix} \beta_x \\ \beta_y \\ 0 \end{Bmatrix} \tag{2}$$

where $\widehat{u}$, $\widehat{v}$, and $\widehat{w}$ represent the displacements along x-, y- and z-axes, respectively; β_x and β_y are two rotations; notations "$_{,x}$" and "$_{,y}$" indicate the partial derivatives respect to x and y, respectively.

The function $f(z)$ describes variation of the shear stress through the

Table 1
The first natural frequency of the flexoelectric square nanoplate (h = 20 nm).

BCs	f_{14} (C/m)	Theory	a/h					
			10	20	30	40	50	100
SSSS	0	Present	5.9069	6.0802	6.1144	6.1266	6.1322	6.1398
		TSDT [35]	5.9069	6.0802	6.1144	6.1266	6.1322	6.1398
		ESDT [36]	5.9365	6.0884	6.1181	6.1287	6.1336	6.1401
	10^{-7}	Present	6.2458	6.4410	6.4798	6.4935	6.4999	6.5085
		TSDT [35]	6.2458	6.4410	6.4798	6.4935	6.4999	6.5085
		ESDT [36]	6.2727	6.4486	6.4832	6.4955	6.5012	6.5088
CCCC	0	Present	10.0488	10.8591	11.0413	11.1086	11.1404	11.1836
		TSDT [35]	10.0488	10.8591	11.0413	11.1086	11.1404	11.1836
		ESDT [36]	10.1929	10.9078	11.0647	11.1221	11.1492	11.1858
	10^{-7}	Present	10.5845	11.4863	11.6924	11.7689	11.8051	11.8543
		TSDT [35]	10.5845	11.4863	11.6924	11.7689	11.8051	11.8543
		ESDT [36]	10.7041	11.5301	11.7138	11.7813	11.8132	11.8564
SCSC	0	Present	8.2437	8.7906	8.9089	8.9520	8.9722	8.9997
		TSDT [35]	8.2437	8.7906	8.9089	8.9520	8.9722	8.9997
		ESDT [36]	8.3420	8.8220	8.9237	8.9605	8.9777	9.0011
	10^{-7}	Present	8.6913	9.3023	9.4363	9.4853	9.5084	9.5396
		TSDT [35]	8.6913	9.3023	9.4363	9.4853	9.5084	9.5396
		ESDT [36]	8.7744	9.3307	9.4499	9.4931	9.5135	9.5409
SFSF	0	Present	2.8569	2.9049	2.9159	2.9204	2.9226	2.9260
		TSDT [35]	2.8569	2.9049	2.9159	2.9204	2.9226	2.9260
		ESDT [36]	2.8647	2.9075	2.9173	2.9213	2.9233	2.9261
	10^{-7}	Present	2.9483	3.0025	3.0155	3.0210	3.0237	3.0279
		TSDT [35]	2.9483	3.0025	3.0155	3.0210	3.0237	3.0279
		ESDT [36]	2.9560	3.0053	3.0171	3.0220	3.0245	3.0281
CFCF	0	Present	6.3155	6.6836	6.7651	6.7959	6.8110	6.8322
		TSDT [35]	6.3155	6.6836	6.7651	6.7959	6.8110	6.8322
		ESDT [36]	6.3841	6.7057	6.7759	6.8024	6.8153	6.8334
	10^{-7}	Present	6.5947	7.0029	7.0959	7.1316	7.1492	7.1744
		TSDT [35]	6.5947	7.0029	7.0959	7.1316	7.1492	7.1744
		ESDT [36]	6.6529	7.0230	7.1060	7.1378	7.1534	7.1755

plate's thickness, adhering to zero shear stress at upper and lower surfaces. This study employs a Chebyshev shear deformation theory grounded in the third-order Chebyshev polynomial, $f(z) = \cos\left(3 \times \cos^{-1}\left(\frac{z}{h}\right)\right)$, inherently fulfilling the zero-shear stress without extra enforcement. Fig. 2 clearly presents the through-thickness distributions of $f(z)$ and its derivative $f'(z) = \frac{\mathrm{d}f(z)}{\mathrm{d}z}$. It can be observed that the derivative naturally vanishes at the top and bottom surfaces $\left(\frac{z}{h} = \pm 0.5\right)$, confirming that the proposed shear function fulfills the zero-shear stress requirement.

The linear bending and shear strain tensor are determined as follows

$$\boldsymbol{\varepsilon} = \begin{Bmatrix} \boldsymbol{\varepsilon}_b \\ \boldsymbol{\varepsilon}_s \end{Bmatrix} = \begin{Bmatrix} \boldsymbol{\varepsilon}_1 + z\boldsymbol{\varepsilon}_2 + f(z)\boldsymbol{\varepsilon}_3 \\ f'(z)\overline{\boldsymbol{\varepsilon}}_s \end{Bmatrix} \tag{3}$$

where

$$\boldsymbol{\varepsilon}_b = \begin{Bmatrix} \varepsilon_{xx} \\ \varepsilon_{yy} \\ \gamma_{xy} \end{Bmatrix};\ \boldsymbol{\varepsilon}_s = \begin{Bmatrix} \gamma_{xz} \\ \gamma_{yz} \end{Bmatrix};\ \boldsymbol{\varepsilon}_1 = \begin{Bmatrix} u_{,x} \\ v_{,y} \\ u_{,y} + v_{,x} \end{Bmatrix};\ \boldsymbol{\varepsilon}_2 = -\begin{Bmatrix} w_{,xx} \\ w_{,yy} \\ 2w_{,xy} \end{Bmatrix};\ \boldsymbol{\varepsilon}_3 = \begin{Bmatrix} \beta_{x,x} \\ \beta_{y,y} \\ \beta_{x,y} + \beta_{y,x} \end{Bmatrix};\ \overline{\boldsymbol{\varepsilon}}_s = \begin{Bmatrix} \beta_x \\ \beta_y \end{Bmatrix} \tag{4}$$

The strain gradient tensor η_{jkl} is defined [49]

$$\eta_{jkl} = \varepsilon_{jk,l} \tag{5}$$

For simplicity, only the thickness-direction strain gradients η_{xxz} and η_{yyz} are considered, as the others are either associated with zero or negligible flexoelectric coefficients [49]. Eq. (5) is rewritten in compact form as follows

$$\boldsymbol{\eta} = \boldsymbol{\eta}_1 + f'(z)\boldsymbol{\eta}_2 \tag{6}$$

where

$$\boldsymbol{\eta} = \begin{Bmatrix} \eta_{xxz} \\ \eta_{yyz} \end{Bmatrix};\ \boldsymbol{\eta}_1 = -\begin{Bmatrix} w_{,xx} \\ w_{,yy} \end{Bmatrix};\ \boldsymbol{\eta}_2 = \begin{Bmatrix} \beta_{x,x} \\ \beta_{y,y} \end{Bmatrix} \tag{7}$$

2.2. The constitutive relations

For nanoscale dielectric materials taking into account the flexoelectric effect, the constitutive equations are formulated as follows [49–51]

$$\begin{cases} \sigma_{ik} = C_{ijkl}\varepsilon_{kl} - e_{kij}E_k \\ \tau_{ijm} = -f_{kijm}E_k \\ D_i = e_{ijk}\varepsilon_{jk} + k_{ij}E_j + f_{ijkl}\eta_{jkl} \end{cases} \tag{8}$$

where σ_{ij}, τ_{ijm}, and D_i represent stress tensor, higher-order stress component tensor and electric displacement, respectively. C_{ijkl}, k_{ij} and e_{kij} denote elastic constant, permittivity and piezoelectric constant, respectively. f_{ijkl} is the tensor representing the coupling between the electric field and strain gradient, accounting for higher-order electromechanical interactions and E_i represents the vector of electric field. The electric field components in the x- and y-directions are assumed to be negligible $E_x = E_y = 0$ [49]. In the present model, only the dominant curvature-related strain gradients η_{xxz} and η_{yyz} are included, as they contribute most significantly to the flexoelectric response. Other gradient terms are omitted because their associated coefficients vanish under transverse isotropy or their effects are negligible compared to the primary bending gradients. Considering that D_x and D_y are sufficiently small compared to D_z, we neglect D_x and D_y while retaining D_z. For the strain gradient, only the components along the thickness direction (η_{xxz} and η_{yyz}) are considered, while others are ignored since the corresponding flexoelectric coefficients are either zero or their magnitudes are much smaller compared with those in the thickness direction. These assumptions are widely adopted in plate and nanoplate models [49], and they simplify the formulation without significantly affecting the accuracy of the predicted deflection and frequency responses. According to

Table 2
The impact of the aspect ratio on the lowest six non-dimensional natural frequencies of the flexoelectric rectangular nanoplate with various BCs ($h = 10$ nm, $a/h = 10$).

BCs	f_{14} (C/m)	Mode	b/a				
			1	1.5	2	2.5	3
SSSS	0	1	5.9069	4.3109	3.7446	3.4810	3.3375
		2	14.0191	8.0888	5.9070	4.8765	4.3110
		3	14.0191	12.5758	9.3870	7.1496	5.9076
		4	21.4226	14.0229	12.0648	10.2342	8.0944
		5	26.0512	15.9995	14.0191	11.8272	10.8404
		6	26.0512	21.4252	14.0351	13.0867	11.6979
	10^{-7}	1	7.1492	5.2310	4.5481	4.2298	4.0564
		2	16.7782	9.7576	7.1493	5.9118	5.2311
		3	16.7782	15.0779	11.3028	8.6368	7.1501
		4	25.4357	16.7833	14.4747	12.3096	9.7651
		5	30.8086	19.1040	16.7783	14.1940	13.0315
		6	30.8086	25.4392	16.7998	15.6803	14.0412
CCCC	0	1	10.0488	7.7055	7.0483	6.7938	6.6719
		2	19.1331	11.5862	9.0105	7.9282	7.3979
		3	19.1331	17.4646	12.4278	9.9864	8.7310
		4	26.8072	17.7706	16.9581	12.9635	10.7199
		5	31.5867	20.6751	17.1244	16.7429	13.3542
		6	31.8622	25.6976	18.6555	16.7820	16.6322
	10^{-7}	1	11.9838	9.2232	8.4433	8.1409	7.9961
		2	22.5919	13.8058	10.7715	9.4886	8.8585
		3	22.5919	20.6480	14.8081	11.9307	10.4433
		4	31.5063	21.0498	20.0560	15.4486	12.8031
		5	37.0293	24.3973	20.3206	19.8042	15.9202
		6	37.3666	28.4178	22.0428	19.9431	19.6746
SCSC	0	1	8.2437	7.1708	6.8366	6.6912	6.6150
		2	15.1423	9.9303	8.2438	7.5309	7.1708
		3	18.2548	15.1459	11.0128	9.1801	8.2442
		4	24.2557	17.2091	15.1572	11.7418	9.9350
		5	26.6308	19.7690	16.8523	15.1867	12.2722
		6	31.2303	22.4304	18.2548	16.6891	15.2543
	10^{-7}	1	9.8660	8.5877	8.1907	8.0183	7.9280
		2	18.0447	11.8753	9.8661	9.0164	8.5877
		3	21.5789	18.0494	13.1623	10.9822	9.8667
		4	28.6076	20.3514	18.0648	14.0282	11.8815
		5	31.4560	23.3560	19.9328	18.1051	14.6600
		6	36.4699	26.5811	21.5789	19.7414	18.1987

Table 3
The lowest six normalized frequencies of the flexoelectric circular nanoplate ($h = 10$ nm).

BCs	f_{14} (C/m)	Mode	R/h					
			10	20	30	40	50	100
SS	0	1	1.5654	1.5767	1.5789	1.5789	1.5796	1.5804
		2	4.2423	4.3315	4.3491	4.3491	4.3554	4.3623
		3	4.2423	4.3315	4.3491	4.3491	4.3554	4.3623
		4	7.5953	7.8943	7.9564	7.9564	7.9790	8.0035
		5	7.6266	7.9052	7.9614	7.9614	7.9815	8.0046
		6	8.7750	9.1484	9.2244	9.2244	9.2515	9.2812
	10^{-7}	1	2.0065	2.0262	2.0299	2.0313	2.0319	2.0327
		2	5.2357	5.3751	5.4028	5.4127	5.4174	5.4236
		3	5.2357	5.3751	5.4028	5.4127	5.4174	5.4236
		4	9.2579	9.7061	9.7998	9.8338	9.8499	9.8717
		5	9.2911	9.7175	9.8059	9.8378	9.8527	9.8728
		6	10.6524	11.222	11.3415	11.3845	11.4046	11.4317
CC	0	1	3.0844	3.1543	3.1679	3.1727	3.1750	3.1779
		2	6.2491	6.5173	6.5717	6.5912	6.6003	6.6125
		3	6.2491	6.5173	6.5717	6.5912	6.6003	6.6125
		4	9.9506	10.6012	10.7396	10.7897	10.8132	10.8448
		5	9.9723	10.6108	10.7469	10.7961	10.8193	10.8504
		6	11.2780	12.0706	12.2407	12.3024	12.3314	12.3704
	10^{-7}	1	3.7394	3.8478	3.8694	3.8771	3.8807	3.8855
		2	7.5278	7.9340	8.0193	8.0501	8.0645	8.0840
		3	7.5278	7.9340	8.0193	8.0501	8.0645	8.0840
		4	11.9169	12.8767	13.0910	13.1695	13.2066	13.2568
		5	11.9416	12.8895	13.1007	13.1782	13.2147	13.2641
		6	13.4871	14.6543	14.9175	15.0142	15.0599	15.1217

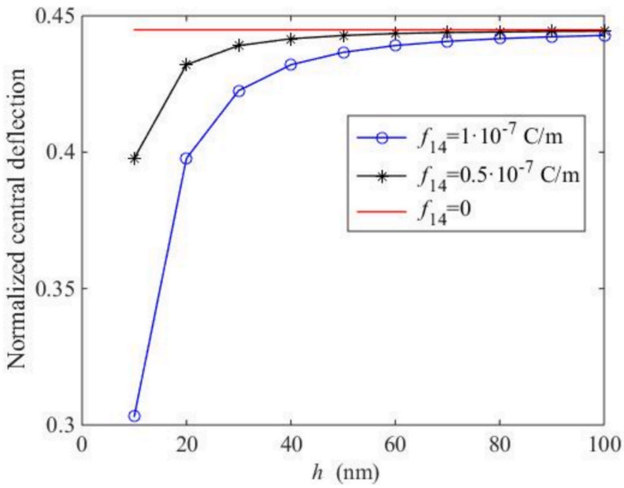

Fig. 6. The normalized deflection of the SSSS flexoelectric square nanoplate under uniform distributed load ($a/h = 10$).

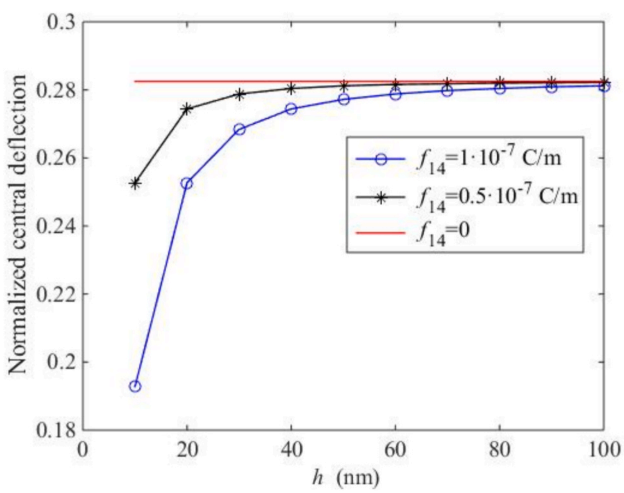

Fig. 7. The normalized deflection of the SSSS flexoelectric square nanoplate subjected to sinusoidal distributed load ($a/h = 10$).

Eqs. (8) and (5), the constitutive equations are rewritten as follows

$$\begin{gathered}
\begin{Bmatrix}\sigma_{xx}\\ \sigma_{yy}\\ \sigma_{xy}\end{Bmatrix}=\begin{bmatrix}C_{11} & C_{12} & 0\\ C_{12} & C_{22} & 0\\ 0 & 0 & C_{66}\end{bmatrix}\begin{Bmatrix}\varepsilon_{xx}\\ \varepsilon_{yy}\\ \gamma_{xy}\end{Bmatrix}-\begin{Bmatrix}e_{31}\\ e_{31}\\ 0\end{Bmatrix}E_z\\
\begin{Bmatrix}\sigma_{xz}\\ \sigma_{yz}\end{Bmatrix}=\begin{bmatrix}C_{66} & 0\\ 0 & C_{66}\end{bmatrix}\begin{Bmatrix}\gamma_{xz}\\ \gamma_{yz}\end{Bmatrix}\\
\begin{Bmatrix}\tau_{xxz}\\ \tau_{yyz}\end{Bmatrix}=-\begin{Bmatrix}f_{14}\\ f_{14}\end{Bmatrix}E_z\\
D_z=e_{31}\left(\varepsilon_{xx}+\varepsilon_{yy}\right)+k_{33}E_z+f_{14}\left(\eta_{xxz}+\eta_{yyz}\right)
\end{gathered} \tag{9}$$

In Eq. (9), the constitutive equations are presented in the general tensorial form. In the subsequent explanation, to simplify the formulation and reflect the assumed material properties, we adopt the Voigt notation under the assumption of transverse isotropy. Accordingly, the general tensor components reduce to the simplified constants: $C_{1111} = C_{2222} = C_{11}$, $C_{1122} = C_{2211} = C_{12}$, $C_{1212} = C_{66}$, and $e_{311} = e_{322} = e_{31}$. Besides, the flexoelectric coefficients are expressed as $f_{3113} = f_{14}$ and $f_{3223} = f_{14}$, as stated in ref. [52].

In compact form, Eq. (9) can be rewritten as follows

$$\begin{cases}\boldsymbol{\sigma}_b=\mathbf{C}_b\boldsymbol{\varepsilon}_b-\mathbf{C}_eE_z\\ \boldsymbol{\sigma}_s=\mathbf{C}_s\boldsymbol{\varepsilon}_s\\ \boldsymbol{\tau}=\mathbf{C}_fE_z\\ D_z=e_{31}\left(\varepsilon_{xx}+\varepsilon_{yy}\right)+k_{33}E_z+f_{14}\left(\eta_{xxz}+\eta_{yyz}\right)\end{cases} \tag{10}$$

where

$$\begin{gathered}
\boldsymbol{\sigma}_b=\begin{Bmatrix}\sigma_{xx}\\ \sigma_{yy}\\ \sigma_{xy}\end{Bmatrix};\ \boldsymbol{\sigma}_s=\begin{Bmatrix}\sigma_{xz}\\ \sigma_{yz}\end{Bmatrix};\ \boldsymbol{\tau}=\begin{Bmatrix}\tau_{xxz}\\ \tau_{yyz}\end{Bmatrix};\ \mathbf{C}_f=\begin{Bmatrix}-f_{14}\\ -f_{14}\end{Bmatrix}\\
\mathbf{C}_b=\begin{bmatrix}C_{11} & C_{12} & 0\\ C_{12} & C_{22} & 0\\ 0 & 0 & C_{66}\end{bmatrix};\ \mathbf{C}_s=\begin{bmatrix}C_{66} & 0\\ 0 & C_{66}\end{bmatrix};\ \mathbf{C}_e=\begin{Bmatrix}e_{31}\\ e_{31}\\ 0\end{Bmatrix}
\end{gathered} \tag{11}$$

The relationship between electric potential and electric field is described as follows

$$E_z=-\frac{\partial\varphi}{\partial z} \tag{12}$$

Without free electric charges, the Gaussian law for electrostatics is expressed as $\nabla\cdot\mathbf{D} = 0$, which, under the above assumptions, reduces to

$$\frac{\partial D_z}{\partial z}=0 \tag{13}$$

Replacing Eqs. (9) and (12) into Eq. (13), we have

$$\varphi_{,zz}=-\frac{e_{31}\left(\varepsilon_x+\varepsilon_y\right)+f_{14}\left(\varepsilon_{x,z}+\varepsilon_{y,z}\right)}{k_{33}} \tag{14}$$

Integrating Eq. (14) with respect to z and inserting it into Eq. (12) yields the function E_z as follows

$$E_z=-\int\frac{e_{31}\left(\varepsilon_x+\varepsilon_y\right)+f_{14}\left(\varepsilon_{x,z}+\varepsilon_{y,z}\right)}{k_{33}}\mathrm{d}z+C \tag{15}$$

where C is the integration constant. In open-circuit conditions, the electric displacement at the surfaces is zero, and is given by

$$D_z\left(z=\pm\frac{h}{2}\right)=0 \tag{16}$$

Substituting E_z from Eq. (15) into D_z in Eq. (9), then substituting into Eq. (16), the integration constant C can be found as follows

$$C=\frac{e_{31}\left(u_{,x}+v_{,y}\right)-f_{14}\left(w_{,xx}+w_{,yy}\right)}{k_{33}} \tag{17}$$

Substituting Eq. (17) into Eq. (15) yields the electric as

$$E_z=g_1(z)E_1+g_2(z)E_2+g_3(z)E_3 \tag{18}$$

where

$$\begin{gathered}
E_1=u_{,x}+v_{,y};\ E_2=w_{,xx}+w_{,yy};\ E_3=\beta_{x,x}+\beta_{y,y}\\
g_1(z)=-\frac{e_{31}}{k_{33}};\ g_2(z)=\frac{f_{14}+e_{31}z}{k_{33}};\ g_3(z)=-\frac{e_{31}f(z)+f_{14}f'(z)}{k_{33}}
\end{gathered} \tag{19}$$

2.3. Hamilton's principle

The equation motion of the smart piezoelectric nanoplate is derived using Hamiltonian principle and expressed [53]

$$\int_{t_1}^{t_2}(\delta K-\delta U-\delta W)\mathrm{d}t \tag{20}$$

where δU, δK and δW, respectively, represent the virtual strain energy, kinetic energy and work done by the external loads.

The virtual strain energy under open-circuit conditions is expressed

Table 4
The normalized deflection of the flexoelectric square nanoplate under uniform distributed load (h = 10 nm).

BCs	f_{14} (C/m)	Theory	a/h					
			10	20	30	40	50	100
SSSS	0	Present	0.4449	0.4259	0.4224	0.4211	0.4206	0.4198
		TSDT [35]	0.4449	0.4259	0.4224	0.4211	0.4206	0.4198
		ESDT [36]	0.4407	0.4248	0.4219	0.4209	0.4204	0.4198
	10^{-7}	Present	0.3032	0.2863	0.2831	0.2820	0.2815	0.2808
		TSDT [35]	0.3032	0.2863	0.2831	0.2820	0.2815	0.2808
		ESDT [36]	0.3018	0.2859	0.2830	0.2819	0.2815	0.2808
SCSC	0	Present	0.2307	0.2065	0.2018	0.2001	0.1994	0.1983
		TSDT [35]	0.2307	0.2065	0.2018	0.2001	0.1994	0.1983
		ESDT [36]	0.2255	0.2051	0.2012	0.1998	0.1991	0.1983
	10^{-7}	Present	0.1606	0.1399	0.1358	0.1343	0.1337	0.1327
		TSDT [35]	0.1606	0.1399	0.1358	0.1343	0.1337	0.1327
		ESDT [36]	0.1597	0.1395	0.1356	0.1342	0.1336	0.1327
SFSF	0	Present	1.4326	1.3991	1.3924	1.3899	1.3887	1.3870
		TSDT [35]	1.4326	1.3991	1.3924	1.3899	1.3887	1.3870
		ESDT [36]	1.4254	1.3972	1.3915	1.3894	1.3883	1.3869
	10^{-7}	Present	1.1064	1.0702	1.0619	1.0584	1.0567	1.0541
		TSDT [35]	1.1064	1.0702	1.0619	1.0584	1.0567	1.0541
		ESDT [36]	1.1022	1.0686	1.0609	1.0578	1.0563	1.0540
CFCF	0	Present	0.3042	0.2740	0.2683	0.2663	0.2653	0.2641
		TSDT [35]	0.3042	0.2740	0.2683	0.2663	0.2653	0.2641
		ESDT [36]	0.2977	0.2723	0.2676	0.2659	0.2651	0.2640
	10^{-7}	Present	0.2150	0.1882	0.1829	0.1810	0.1801	0.1788
		TSDT [35]	0.2150	0.1882	0.1829	0.1810	0.1801	0.1788
		ESDT [36]	0.2138	0.1877	0.1826	0.1808	0.1800	0.1788

Table 5
The normalized deflection of the flexoelectric square nanoplate under sinusoidal distributed load (h = 10 nm).

BCs	f_{14} (C/m)	a/h					
		10	20	30	40	50	100
SSSS	0	0.2825	0.2694	0.2670	0.2661	0.2658	0.2652
	10^{-7}	0.1928	0.1812	0.1790	0.1783	0.1779	0.1774
SCSC	0	0.1566	0.1403	0.1372	0.1360	0.1355	0.1348
	10^{-7}	0.1091	0.0951	0.0923	0.0913	0.0909	0.0902
SFSF	0	0.7329	0.7138	0.7101	0.7087	0.7081	0.7072
	10^{-7}	0.5527	0.5332	0.5290	0.5273	0.5264	0.5252
CFCF	0	0.1873	0.1683	0.1647	0.1634	0.1628	0.1619
	10^{-7}	0.1314	0.1148	0.1115	0.1103	0.1097	0.1090

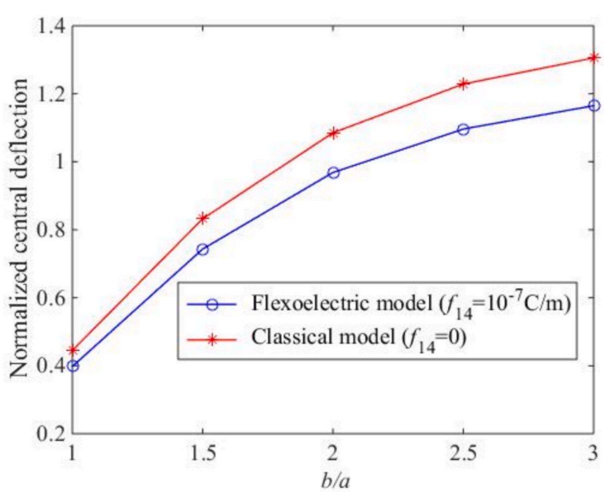

Fig. 8. The normalized central deflection of the SSSS flexoelectric rectangular nanoplates under subjected to the uniform distributed load (h = 20 nm, a/h = 10).

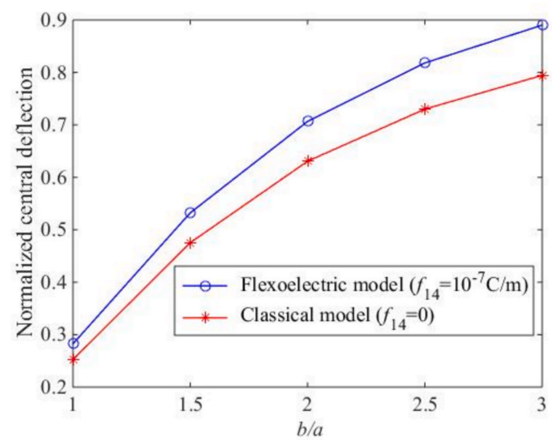

Fig. 9. The normalized central deflection of the SSSS flexoelectric rectangular nanoplate subjected to the sinusoidal distributed load (h = 20 nm, a/h = 10).

Table 6
The normalized deflection of the flexoelectric circular nanoplate under the uniform distributed load (h = 20 nm).

BCs	f_{14} (C/m)	R/h					
		10	20	30	40	50	100
SS	0	6.3066	6.2425	6.2306	6.2264	6.2245	6.2219
	10^{-7}	5.4300	5.3687	5.3573	5.3533	5.3515	5.3490
CC	0	1.6967	1.6345	1.6229	1.6188	1.6169	1.6144
	10^{-7}	1.5156	1.4560	1.4448	1.4409	1.4391	1.4366

$$\delta U = \int_V \left(\delta\boldsymbol{\varepsilon}_b^T\boldsymbol{\sigma}_b + \delta\boldsymbol{\varepsilon}_s^T\boldsymbol{\sigma}_s - \delta E_z D_z + \delta\boldsymbol{\eta}^T\boldsymbol{\tau}\right)\mathrm{d}V \tag{21}$$

Substituting Eqs. (3), (6), (10) and (18) into Eq. (21), the virtual strain energy is expressed

$$\delta U = \int_\Omega \left(\delta\bar{\boldsymbol{\varepsilon}}_b^T\overline{\mathbf{D}}_b\bar{\boldsymbol{\varepsilon}}_b + \delta\bar{\boldsymbol{\varepsilon}}_s^T\overline{\mathbf{D}}_s\bar{\boldsymbol{\varepsilon}}_s - \delta\bar{\boldsymbol{\varepsilon}}_b^T\overline{\mathbf{D}}_{me}\overline{\mathbf{E}} + \delta\boldsymbol{\eta}^T\overline{\mathbf{D}}_f\overline{\mathbf{E}}\right)\mathrm{d}\Omega \tag{22}$$

where

$$\overline{\boldsymbol{\varepsilon}}_b=\begin{Bmatrix}\boldsymbol{\varepsilon}_1\\ \boldsymbol{\varepsilon}_2\\ \boldsymbol{\varepsilon}_3\end{Bmatrix};\ \overline{\boldsymbol{\eta}}=\begin{Bmatrix}\boldsymbol{\eta}_1\\ \boldsymbol{\eta}_2\end{Bmatrix};\ \overline{\mathbf{E}}=\begin{Bmatrix}E_1\\ E_2\\ E_3\end{Bmatrix}$$

$$\overline{\mathbf{D}}_b=\begin{bmatrix}\mathbf{A}^b & \mathbf{B}^b & \mathbf{E}^b\\ \mathbf{B}^b & \mathbf{D}^b & \mathbf{F}^b\\ \mathbf{E}^b & \mathbf{F}^b & \mathbf{H}^b\end{bmatrix};\ \overline{\mathbf{D}}_{me}=\begin{bmatrix}\mathbf{A}_{ue} & \mathbf{B}_{ue} & \mathbf{C}_{ue}\\ \mathbf{D}_{ue} & \mathbf{E}_{ue} & \mathbf{F}_{ue}\\ \mathbf{G}_{ue} & \mathbf{H}_{ue} & \mathbf{I}_{ue}\end{bmatrix};\ \overline{\mathbf{D}}_f=\begin{bmatrix}\mathbf{A}_h & \mathbf{B}_h & \mathbf{C}_h\\ \mathbf{D}_h & \mathbf{E}_h & \mathbf{F}_h\end{bmatrix}$$

$$\left(\mathbf{A}^b,\mathbf{B}^b,\mathbf{D}^b,\mathbf{E}^b,\mathbf{F}^b,\mathbf{H}^b\right)=\int_{-h/2}^{h/2}\left(1,z,z^2,f(z),zf(z),f^2(z)\right)\mathbf{C}_b\mathrm{d}z$$

$$\overline{\mathbf{D}}_s=\int_{-h/2}^{h/2}f^{'}(z)\mathbf{C}_s\mathrm{d}z$$

$$\left(\mathbf{A}_{ue},\mathbf{B}_{ue},\mathbf{C}_{ue},\mathbf{D}_{ue},\mathbf{E}_{ue},\mathbf{F}_{ue}\right)=\int_{-h/2}^{h/2}\left(g_1(z),g_2(z),g_3(z),zg_1(z),zg_2(z),zg_3(z)\right)\mathbf{C}_e\mathrm{d}z$$

$$\left(\mathbf{G}_{ue},\mathbf{H}_{ue},\mathbf{I}_{ue}\right)=\int_{-h/2}^{h/2}\left(f(z)g_1(z),f(z)g_2(z),f(z)g_3(z)\right)\mathbf{C}_e\mathrm{d}z$$

$$\left(\mathbf{A}_h,\mathbf{B}_h,\mathbf{C}_h,\mathbf{D}_h,\mathbf{E}_h,\mathbf{F}_h\right)=\int_{-h/2}^{h/2}\left(g_1(z),g_2(z),g_3(z),f^{'}(z)g_1(z),f^{'}(z)g_2(z),f^{'}(z)g_3(z)\right)\mathbf{C}_f\mathrm{d}z \tag{23}$$

The variation of kinetic energy is described

$$\delta K=\int_\Omega\delta\overline{\mathbf{u}}^T\mathbf{I}_m\ddot{\overline{\mathbf{u}}}\mathrm{d}\Omega \tag{24}$$

in which

$$\overline{\mathbf{u}}=\begin{Bmatrix}\mathbf{u}_1\\ \mathbf{u}_2\\ \mathbf{u}_3\end{Bmatrix};\ \mathbf{u}_1=\begin{Bmatrix}u\\ v\\ w\end{Bmatrix};\ \mathbf{u}_2=-\begin{Bmatrix}w_{,x}\\ w_{,y}\\ 0\end{Bmatrix};\ \mathbf{u}_3=\begin{Bmatrix}\beta_x\\ \beta_y\\ 0\end{Bmatrix};\ \mathbf{I}_m=\begin{bmatrix}\mathbf{I}_0 & 0 & 0\\ 0 & \mathbf{I}_0 & 0\\ 0 & 0 & \mathbf{I}_0\end{bmatrix};\ \mathbf{I}_0=\begin{bmatrix}I_1 & I_2 & I_4\\ I_2 & I_3 & I_5\\ I_4 & I_5 & I_6\end{bmatrix}$$

$$\left(I_1,I_2,I_3,I_4,I_5,I_6\right)=\int_{-h/2}^{h/2}\left(1,z,z^2,f(z),zf(z),f^2(z)\right)\rho\mathrm{d}z \tag{25}$$

Furthermore, the variation of the work performed by the external load is given

$$\delta W=\int_\Omega f_0\delta w\mathrm{d}\Omega \tag{26}$$

where f_0 denote the transverse distributed load.

By replacing Eqs. (22), (24) and (26) into Eq. (20), the weak form of the piezoelectric nanoplate is reformulated as

$$\int_\Omega\left(\delta\overline{\boldsymbol{\varepsilon}}_b^T\overline{\mathbf{D}}_b\overline{\boldsymbol{\varepsilon}}_b+\delta\overline{\boldsymbol{\varepsilon}}_s^T\overline{\mathbf{D}}_s\overline{\boldsymbol{\varepsilon}}_s-\delta\overline{\boldsymbol{\varepsilon}}_b^T\overline{\mathbf{D}}_{me}\overline{\mathbf{E}}+\delta\overline{\boldsymbol{\eta}}^T\overline{\mathbf{D}}_f\overline{\mathbf{E}}\right)\mathrm{d}\Omega-\int_\Omega\delta\overline{\mathbf{u}}^T\mathbf{I}_m\ddot{\overline{\mathbf{u}}}\mathrm{d}\Omega=\int_\Omega f_0\delta w\mathrm{d}\Omega \tag{27}$$

2.4. A NURBS based formulation of the piezoelectric nanoplate

The displacement fields $\mathbf{u}^h$ are approximated using the NURBS basis functions [41]

$$\mathbf{u}^h(\varsigma,\eta)=\sum_{i=1}^{m\times n}\mathbf{N}_i(\varsigma,\eta)\mathbf{d}_i \tag{28}$$

In this expression, $\mathbf{d}_i=\left\{u_i\ \ v_i\ \ w_i\ \ \beta_{xi}\ \ \beta_{yi}\right\}^T$, $\mathbf{N}_i(\varsigma,\eta)$ describes the NURBS shape function, which is defined as follows

$$\mathbf{N}_i(\varsigma,\eta)=\begin{bmatrix}N_i(\varsigma,\eta) & 0 & 0 & 0 & 0\\ 0 & N_i(\varsigma,\eta) & 0 & 0 & 0\\ 0 & 0 & N_i(\varsigma,\eta) & 0 & 0\\ 0 & 0 & 0 & N_i(\varsigma,\eta) & 0\\ 0 & 0 & 0 & 0 & N_i(\varsigma,\eta)\end{bmatrix} \tag{29}$$

The strains are reconstructed by replacing Eq. (28) into Eqs. (4) and (23), as shown

$$\overline{\boldsymbol{\varepsilon}}_b=\sum_{i=1}^{m\times n}\begin{Bmatrix}\mathbf{B}_{b1i}\\ \mathbf{B}_{b2i}\\ \mathbf{B}_{b3i}\end{Bmatrix}\mathbf{d}_i=\sum_{i=1}^{m\times n}\overline{\mathbf{B}}_{bi}\mathbf{d}_i;\quad \overline{\boldsymbol{\varepsilon}}_s=\sum_{i=1}^{m\times n}\overline{\mathbf{B}}_{si}\mathbf{d}_i \tag{30}$$

in which

$$\mathbf{B}_{b1i}=\begin{bmatrix}N_{i,x} & 0 & 0 & 0 & 0\\ 0 & N_{i,y} & 0 & 0 & 0\\ N_{i,y} & N_{i,x} & 0 & 0 & 0\end{bmatrix};\ \mathbf{B}_{b2i}=-\begin{bmatrix}0 & 0 & N_{i,xx} & 0 & 0\\ 0 & 0 & N_{i,yy} & 0 & 0\\ 0 & 0 & 2N_{i,xy} & 0 & 0\end{bmatrix};\ \mathbf{B}_{b3i}=\begin{bmatrix}0 & 0 & 0 & N_{i,x} & 0\\ 0 & 0 & 0 & 0 & N_{i,y}\\ 0 & 0 & 0 & N_{i,y} & N_{i,x}\end{bmatrix};\ \overline{\mathbf{B}}_{si}=\begin{bmatrix}0 & 0 & 0 & N_i & 0\\ 0 & 0 & 0 & 0 & N_i\end{bmatrix} \tag{31}$$

The strain gradient and electric field after substituting Eq. (28) into Eq. (23) are given as

$$\overline{\boldsymbol{\eta}}=\begin{Bmatrix}\mathbf{B}_{\eta1i}\\ \mathbf{B}_{\eta2i}\end{Bmatrix}\mathbf{d}_i=\sum_{i=1}^{m\times n}\overline{\mathbf{B}}_{\eta i}\mathbf{d}_i\overline{\mathbf{E}}=\sum_{i=1}^{m\times n}\begin{Bmatrix}\mathbf{B}_{e1i}\\ \mathbf{B}_{e2i}\\ \mathbf{B}_{e3i}\end{Bmatrix}\mathbf{d}_i=\sum_{i=1}^{m\times n}\overline{\mathbf{B}}_{ei}\mathbf{d}_i \tag{32}$$

where

$$\mathbf{B}_{\eta 1i} = \begin{bmatrix} 0 & 0 & -N_{i,xx} & 0 & 0 \\ 0 & 0 & -N_{i,xx} & 0 & 0 \end{bmatrix};\ \mathbf{B}_{\eta 2i} = \begin{bmatrix} 0 & 0 & 0 & N_{i,x} & 0 \\ 0 & 0 & 0 & 0 & N_{i,y} \end{bmatrix};\ \mathbf{B}_{e1i} = \left\{ N_{i,x} \quad N_{i,y} \quad 0 \quad 0 \quad 0 \right\}$$

$$\mathbf{B}_{e2i} = \left\{ 0 \quad 0 \quad N_{i,xx} + N_{i,yy} \quad 0 \quad 0 \right\}$$

$$\mathbf{B}_{e3i} = \left\{ 0 \quad 0 \quad 0 \quad -N_{i,x} \quad -N_{i,y} \right\} \tag{33}$$

Furthermore, the displacement vector can be represented

$$\overline{\mathbf{u}} = \begin{Bmatrix} \mathbf{u}_1 \\ \mathbf{u}_2 \\ \mathbf{u}_3 \end{Bmatrix} = \sum_{i=1}^{m\times n} \begin{Bmatrix} \mathbf{N}_{1i} \\ \mathbf{N}_{2i} \\ \mathbf{N}_{3i} \end{Bmatrix} \mathbf{d}_i = \sum_{i=1}^{m\times n} \overline{\mathbf{N}}_i \mathbf{d}_i \tag{34}$$

where

$$\mathbf{N}_{1i} = \begin{bmatrix} N_i & 0 & 0 & 0 & 0 \\ 0 & N_i & 0 & 0 & 0 \\ 0 & 0 & N_i & 0 & 0 \end{bmatrix};\ \mathbf{N}_{2i} = \begin{bmatrix} 0 & 0 & -N_{i,x} & 0 & 0 \\ 0 & 0 & -N_{i,y} & 0 & 0 \\ 0 & 0 & 0 & 0 & 0 \end{bmatrix};\ \mathbf{N}_{3i} = \begin{bmatrix} 0 & 0 & 0 & N_i & 0 \\ 0 & 0 & 0 & 0 & N_i \\ 0 & 0 & 0 & 0 & 0 \end{bmatrix} \tag{35}$$

By substituting Eqs. (30), (32) and (34) into Eq. (27), we obtain

$$\mathbf{Kd} + \mathbf{M}\ddot{\mathbf{d}} = \mathbf{F} \tag{36}$$

where **K** represents the stiffness matrix, formulated as follows

$$\mathbf{K} = \int_\Omega \left(\overline{\mathbf{B}}_b^T \overline{\mathbf{D}}_b \overline{\mathbf{B}}_b + \overline{\mathbf{B}}_s^T \overline{\mathbf{D}}_s \overline{\mathbf{B}}_s - \overline{\mathbf{B}}_b^T \overline{\mathbf{D}}_{me} \overline{\mathbf{B}}_e + \overline{\mathbf{B}}_\eta^T \overline{\mathbf{D}}_f \overline{\mathbf{B}}_e \right) \mathrm{d}\Omega \tag{37}$$

In addition, **M** and **F** respectively represent the mass matrix and force vector as

$$\mathbf{M} = \int_\Omega \overline{\mathbf{N}}^T \mathbf{I}_m \overline{\mathbf{N}} \mathrm{d}\Omega;\ \mathbf{F} = \int_\Omega f_0 \mathbf{B}_F \mathrm{d}\Omega;\ \mathbf{B}_F = \left\{ 0 \quad 0 \quad N_i \quad 0 \quad 0 \right\}^T \tag{38}$$

The free vibration governing equation is expressed as

$$\left(\mathbf{K} - \omega^2 \mathbf{M} \right) \overline{\mathbf{d}} = \mathbf{0} \tag{39}$$

in which $\overline{\mathbf{d}}$ ($\mathbf{d} = \overline{\mathbf{d}} e^{-i\omega t}$) and ω are mode shape and natural frequency.

Similarly, the static governing equation of the smart piezoelectric nanoplate is presented

$$\mathbf{Kd} = \mathbf{F} \tag{40}$$

3. Numerical results

Free vibration and static bending of a smart flexoelectric nanoplate made of PZT-5H material are studied. Material properties are given as [49]: $e_{31} = -17.05$ C/m^2, $k_{33} = 1.76 \times 10^{-8}$ C/(Vm), $C_{11} = 102$ GPa, $C_{66} = 35.5$ GPa, $C_{12} = 31$ GPa and $\rho = 7600$ kg/m^3. Two models, including the classical model (without flexoelectric effect with $f_{14} = 0$) and the flexoelectric model (considering the flexoelectric effect with $f_{14} = 10^{-7}$ C/m), are studied in this section. Besides, for numerical calculations, different boundary conditions (BCs) for the rectangular nanoplates are used and presented as follows.

SSSS

$$\begin{cases} \left(v, w, \beta_y\right)\big|_{x=0,a} = 0 \\ \left(u, w, \beta_x\right)\big|_{y=0,b} = 0 \end{cases} \tag{41}$$

CCCC

$$\begin{cases} \left(u, v, w, w_{,n}, \beta_x, \beta_y\right)\big|_{x=0,a} = 0 \\ \left(u, v, w, w_{,n}, \beta_x, \beta_y\right)\big|_{y=0,b} = 0 \end{cases}$$

SCSC

$$\begin{cases} \left(v, w, \beta_y\right)\big|_{x=0,a} = 0 \\ \left(u, v, w, w_{,n}, \beta_x, \beta_y\right)\big|_{y=0,b} = 0 \end{cases}$$

SSSF

$$\begin{cases} \left(v, w, \beta_y\right)\big|_{x=0,a} = 0 \\ \left(u, w, \beta_x\right)\big|_{y=0} = 0 \end{cases}$$

CCCF

$$\begin{cases} \left(u, v, w, w_{,n}, \beta_x, \beta_y\right)\big|_{x=0,a} = 0 \\ \left(u, v, w, w_{,n}, \beta_x, \beta_y\right)\big|_{y=0} = 0 \end{cases}$$

where the notations “F”, “S” and “C” represent free, simply supported and clamped, respectively.

For circular nanoplates, BCs are expressed.

SS

$$(u, v, w) = 0 \tag{42}$$

CC

$$\left(u, v, w, w_{,n}, \beta_x, \beta_y\right) = 0$$

3.1. Validation

To validate the present method, various examples are examined, and their results are benchmarked against published data. Initially, the free vibration of a smart nanoplate made of PZT-5H material [49] is investigated. The first natural frequency of the flexoelectric piezoelectric rectangular nanoplate under SSSS boundaries is presented in Fig. 3. The present results are compared with the reference solutions provided Yang et al. [49], using the analytical method based on KPT with two variables. As seen in Fig. 3, the numerical results align closely with the reference results for the case of free vibration analysis. Next, static analysis of the SSSS smart nanoplate with flexoelectricity is examined. Fig. 4 presents a comparison of the central deflection of the plate with the reference solution provided by Yang et al. [49]. The results in Fig. 4 closely correspond to those reported in the referenced work. The comparison results in Fig. 3 and Fig. 4 highlight the accuracy and reliability of the proposed model in analyzing the flexoelectric nanoplate.

3.2. Free vibration

We now consider free vibration of smart flexoelectric rectangular and circular nanoplates. For numerical examinations, the normalized natural frequency $\Omega = \frac{\omega a^2}{h}\sqrt{\frac{\rho}{C_{11}}}$ is used for rectangular nanoplate. Fig. 5 depicts the variation of the first normalized natural frequency of piezoelectric square nanoplates with respect to thickness for different flexoelectric coefficients ($f_{14} = 0$, 0.5×10^{-7} and 1×10^{-7}C/m). The flexoelectric effect markedly enhances the natural frequency, particularly for thinner plates, where size-dependent behavior is most pronounced. As the thickness increases, the influence of flexoelectricity gradually weakens, and the results converge toward those of the classical model ($f_{14} = 0$). Moreover, the increase in natural frequency becomes more pronounced with higher values of the flexoelectric coefficient f_{14}, highlighting its crucial role in nanoscale electromechanical behavior. This trend demonstrates that flexoelectricity dominates at the nanoscale but becomes negligible in thicker plates, emphasizing the importance of incorporating it for accurate modeling of nanoscale electromechanical systems. Table 1 presents the lowest six natural frequencies of the piezoelectric square nanoplate. The present results predicted by TCSDT are compared with those derived from TSDT [35] and ESDT [36]. A good correlation is observed between the outcomes of TCSDT and those of TSDT and ESDT. Besides, according to the numerical results in Table 1, a rise in the length-to-thickness ratio makes the natural frequency increasing for both classical and flexoelectric plate models. Moreover, the study reveals that the flexoelectric effect leads to an increase in the first natural frequency of the piezoelectric nanoplate. This increase is primarily due to the strain-gradient-induced polarization that produces an internal electric field that opposes deformation, increasing stored elastic energy and thus the apparent stiffness, especially at the nanoscale. When comparing different boundary conditions, the fully clamped (CCCC) configuration yields the greatest dynamic stiffness due to its complete edge constraints, while the simply supported-free (SFSF) configuration results in the lowest because of its greater flexibility. Furthermore, the influence of the width-to-length ratio on the first six dimensionless natural frequencies is summarized in Table 2. The results clearly demonstrate that as the width-to-length ratio rises, the normalized natural frequencies of the piezoelectric rectangular nanoplates tend to decrease. Table 3 shows the lowest six dimensionless frequencies $\overline{\Omega} = \frac{\omega R^2}{h}\sqrt{\frac{\rho}{C_{11}}}$ of the piezoelectric circular nanoplates with different radius-to-thickness ratios. When the radius-to-thickness ratio increases, the dimensionless vibrational frequency of the circular nanoplate increases as well.

3.3. Static analysis

We now consider bending of the piezoelectric rectangular and circular nanoplates under uniformly and sinusoidal distributed loads. The normalized central deflection ($\overline{w} = \frac{10C_{11}h^3}{f_0 a^4} w\left(\frac{a}{2}, \frac{b}{2}, 0\right)$ for rectangular and $\overline{w}_c = \frac{10C_{11}h^3}{f_0 R^4} w(0,0,0)$ for circular nanoplates) is used for numerical calculation. The effect of the piezoelectric coefficient (f_{14}) and thickness (h) on the normalized central deflection $\overline{w}$ of the SSSS piezoelectric square nanoplates under uniform and sinusoidal distributed loads is illustrated in Fig. 6 and Fig. 7, respectively. The horizontal axis represents the plate thickness, while the vertical axis denotes the normalized central deflection $\overline{w}$. As the piezoelectric coefficient increases, the deflection of the nanoplate decreases due to enhanced electromechanical coupling. Moreover, the deflection predicted by the flexoelectric model gradually converges to the classical result as the plate thickness increases. It is also observed that the flexoelectric effect notably reduces the normalized deflection, particularly for thinner plates, where size-dependent behavior becomes significant. Furthermore, the impact of both the length-to-thickness ratio and boundary conditions on the normalized central deflection of piezoelectric square nanoplates, subjected to uniform and sinusoidal distributed loads, is examined and summarized in Table 4 and Table 5, respectively. The results presented in these tables reveal that an increase in the length-to-thickness ratio leads to a noticeable decrease in the deflection of the nanoplate. In Table 4, the normalized deflection obtained by the present method using both TCSDT, TSDT [35] and ESDT [36] is compared. The comparison in Table 4 demonstrates that the TCSDT results are consistent with TSDT and align closely with ESDT. TCSDT and TSDT produce similar results. Fig. 8 and Fig. 9 plot effect of the width-to-length ratio (b/a) on the normalized deflection of the SSSS piezoelectric nanoplate subjected to uniform and sinusoidal distributed loads, respectively. In both figures, the horizontal axis represents the geometric ratio b/a, while the vertical axis denotes the normalized central deflection. It is observed that the deflection increases with increasing b/a, and the flexoelectric model predicts smaller deflections than the classical model due to the size-dependent stiffening effect. Lastly, the static bending behavior of flexoelectric piezoelectric circular nanoplates under a uniformly distributed load is investigated for various radius-to-thickness ratios, with the findings summarized in Table 6. The data indicate that as the radius-to-thickness ratio increases, the normalized deflection of the nanoplate steadily decreases.

4. Conclusion

The bending and free vibration of the smart flexoelectric nanoplates were examined. The third-order Chebyshev shear deformation theory was used to derive the displacement fields of the nanoplates. The governing equation of the flexoelectric nanoplate was derived employing the Hamilton principle. The NURBS basic function in IGA was used to approximate the displacement strain, and higher-order strain of the nanoplate. The numerical results agreed with those from a reference, showing the advantage of the proposed method. The effect of flexoelectricity and geometries on the deflection and natural frequencies of the piezoelectric nanoplates was studied. The numerical outcomes show that:

- The results from the third-order Chebyshev shear deformation theory are consistent with TSDT and align closely with those from other shear deformation theories.
- As the plate thickness increases, the flexoelectric model's predictions for natural frequency and deflection approach the classical results. Flexoelectric effects are significant for thin plates but fade as the thickness grows.
- As the length-to-thickness and radius-to-thickness ratios increase, the stiffness of the piezoelectric nanoplate rises in both the classical and flexoelectric plate models.
- The piezoelectric rectangular nanoplate's frequency and deflection decrease and increase as the width-to-length ratio rises.
- This study advances knowledge of the dynamic and static responses of flexoelectric piezoelectric nanoplates and provides valuable guidance for their design in aerospace, mechanical, and smart structural applications.

CRediT authorship contribution statement

P.T. Hung: Writing – original draft, Visualization, Validation, Methodology, Investigation. **H. Nguyen-Xuan:** Writing – review & editing, Visualization, Methodology. **M. Abdel-Wahab:** Writing – review & editing, Visualization, Methodology. **Chien H. Thai:** Writing – review & editing, Writing – original draft, Visualization, Validation, Methodology, Conceptualization. **P. Phung-Van:** Writing – review & editing, Visualization, Validation, Methodology, Funding acquisition.

Declaration of competing interest

The authors declare that they have no known competing financial interests or personal relationships that could have appeared to influence the work reported in this paper.

Acknowledgements

This research is funded by Vietnam National Foundation for Science and Technology Development (NAFOSTED) under grant number 107.02-2023.79.

Data availability

No data was used for the research described in the article.

References

[1] Wang ZL, Song J. Piezoelectric Nanogenerators based on Zinc Oxide Nanowire Arrays. Science 2006;312(5771):242–6.

[2] Yan TH, Chen XD, Dou WF, Lin RM. Feedback control of disk vibration and flutter by distributed felf-sensing piezoceramic actuators. Mech Based Des Struct Mach 2008;36(3):283–305.

[3] Chen J, Li D, Zhang G, Qu Y. Constitutive matrices for 32 typical classes of crystalline solids with couple stress, quadrupole, and curvature-based flexoelectric effects. Acta Mech 2023;234(11):5301–30.

[4] Nye JF. Physical properties of crystals: their representation by tensors and matrices. Oxford University Press; 1985.
[5] Chen J, Qu Y, Guo Z, Li D, Zhang G. A one-dimensional model for mechanical coupling metamaterials using couple stress theory. Math Mech Solids 2023;28(12): 2732–55.
[6] Yan Z, Jiang LY. Vibration and buckling analysis of a piezoelectric nanoplate considering surface effects and in-plane constraints. Proceedings of the Royal Society A: Mathematical, Physical and Engineering Sciences 2012;468(2147): 3458–75.
[7] Yan Z, Jiang LY. Flexoelectric effect on the electroelastic responses of bending piezoelectric nanobeams. J Appl Phys 2013;113(19).
[8] Qu Y, Pan E, Zhu F, Deng Q. A thermodynamically consistent theory for flexoelectronics: Interaction between strain gradient and electric current in flexoelectric semiconductors. Int J Eng Sci 2025;208:104165.
[9] Zhang Z, Yan Z, Jiang L. Flexoelectric effect on the electroelastic responses and vibrational behaviors of a piezoelectric nanoplate. J Appl Phys 2014;116(1): 014307.
[10] Yue YM, Xu KY, Chen T. A micro scale Timoshenko beam model for piezoelectricity with flexoelectricity and surface effects. Compos Struct 2016;136:278–86.
[11] Wang X, Zhang R, Jiang L. A study of the flexoelectric effect on the electroelastic fields of a cantilevered piezoelectric nanoplate. Int J Appl Mech 2017;9(04): 1750056.
[12] Ebrahimi F, Barati MR. Static stability analysis of embedded flexoelectric nanoplates considering surface effects. Appl Phys A 2017;123:1–15.
[13] Ebrahimi F, Barati MR. Vibration analysis of size-dependent flexoelectric nanoplates incorporating surface and thermal effects. Mech Adv Mater Struct 2018; 25(7):611–21.
[14] Ebrahimi F, Barati MR. Dynamic modeling of embedded nanoplate systems incorporating flexoelectricity and surface effects. Microsyst Technol 2019;25(1): 175–87.
[15] Chu L, Dui G, Ju C. Flexoelectric effect on the bending and vibration responses of functionally graded piezoelectric nanobeams based on general modified strain gradient theory. Compos Struct 2018;186:39–49.
[16] Zeng S, Wang BL, Wang KF. Nonlinear vibration of piezoelectric sandwich nanoplates with functionally graded porous core with consideration of flexoelectric effect. Compos Struct 2019;207:340–51.
[17] Amir S, BabaAkbar-Zarei H, Khorasani M. Flexoelectric vibration analysis of nanocomposite sandwich plates. Mech Based Des Struct Mach 2020;48(2):146–63.
[18] Ghorbanpour Arani A, Soltan Arani A, Haghparast E. Flexoelectric and surface effects on vibration frequencies of annular nanoplate. Indian J Phys 2021;95: 2063–83.
[19] El Dhaba AR, Gabr ME. Modeling the flexoelectric effect of an anisotropic dielectric nanoplate. Alex Eng J 2021;60(3):3099–106.
[20] Malikan M, Eremeyev VA. On the dynamics of a visco–piezo–flexoelectric nanobeam. Symmetry 2020;12(4):643.
[21] Wang B, Li X-F. Flexoelectric effects on the natural frequencies for free vibration of piezoelectric nanoplates. J Appl Phys 2021;129(3):034102.
[22] Yu P, Leng W, Peng L, Suo Y, Guo J. The bending and vibration responses of functionally graded piezoelectric nanobeams with dynamic flexoelectric effect. Results Phys 2021;28:104624.
[23] Zhao X, Zheng S, Li Z. Effects of porosity and flexoelectricity on static bending and free vibration of AFG piezoelectric nanobeams. Thin-Walled Struct 2020;151: 106754.
[24] Xu JW, Wang P, Liu ZH. Electromechanical coupling in piezoelectric nanoplate due to the flexoelectric effect. Acta Mech 2024;235(1):479–92.
[25] Zhou S, Li A, Zhang R, Qi L, Ren F, Zheng Z, et al. Electro-mechanical responses of flexoelectric bilayer circular nano-plate with surface effect. Int J Mech Mater Des 2024;20(2):209–31.
[26] Liu Z, Wang P, Xu J. The electro-mechanical coupling responses of functionally graded piezoelectric nanobeams with flexoelectric effect. AIP Adv 2023;13(6): 065221.
[27] Xu J, Wang P, Xiao Z. Dynamic flexoelectric effect on the vibration behavior of piezoelectric nanoplates. Acta Mech 2024.
[28] Nguyen V-L, Nguyen V-L, Tran M-T, Dang X-T. Investigation of static buckling and bending of nanoplates made of new functionally graded materials considering surface effects on an elastic foundation. Acta Mech 2024;235(12):7807–33.
[29] Jearsiripongkul T, Saffari PR, Thongchom C, Lawongkerd J, Saffari PR, Keawsawasvong S, et al. Hygrothermomechanical loading-induced vibration study of multilayer piezoelectric nanoplates with functionally graded porous cores resting on a variable viscoelastic substrate. International Journal of Thermofluids 2024;23:100715.
[30] Zhang M, Guo J. Bending, free vibration and buckling of layered piezoelectric semiconductor nanoplates based on modified couple stress theory. Acta Mech 2024.
[31] Naskar S, Shingare KB, Mondal S, Mukhopadhyay T. Flexoelectricity and surface effects on coupled electromechanical responses of graphene reinforced functionally graded nanocomposites: a unified size-dependent semi-analytical framework. Mech Syst Sig Process 2022;169:108757.
[32] Qu Y, Pan E, Zhu F, Jin F, Roy AK. Modeling thermoelectric effects in piezoelectric semiconductors: New fully coupled mechanisms for mechanically manipulated heat flux and refrigeration. Int J Eng Sci 2023;182:103775.
[33] Qu Y, Zhu F, Pan E, Jin F, Hirakata H. Analysis of wave-particle drag effect in flexoelectric semiconductor plates via Mindlin method. App Math Model 2023;118: 541–55.
[34] Qu YL, Li P, Zhang GY, Jin F, Gao XL. A microstructure-dependent anisotropic magneto-electro-elastic Mindlin plate model based on an extended modified couple stress theory. Acta Mech 2020;231(10):4323–50.
[35] Reddy J. Energy and variational methods in applied mechanics : with an introduction to the finite element method. 1984.
[36] Karama M, Afaq KS, Mistou S. Mechanical behaviour of laminated composite beam by the new multi-layered laminated composite structures model with transverse shear stress continuity. Int J Solids Struct 2003;40(6):1525–46.
[37] Neves AMA, Ferreira AJM, Carrera E, Cinefra M, Roque CMC, Jorge RMN, et al. A quasi-3D hyperbolic shear deformation theory for the static and free vibration analysis of functionally graded plates. Compos Struct 2012;94(5):1814–25.
[38] Zenkour AM. A quasi-3D refined theory for functionally graded single-layered and sandwich plates with porosities. Compos Struct 2018;201:38–48.
[39] Arya H, Shimpi RP, Naik NK. A zigzag model for laminated composite beams. Compos Struct 2002;56(1):21–4.
[40] Shimpi RP. Refined plate theory and its variants. AIAA J 2002;40(1):137–46.
[41] Hughes TJ, Cottrell JA, Bazilevs Y. Isogeometric analysis: CAD, finite elements, NURBS, exact geometry and mesh refinement. Comput Methods Appl Mech Eng 2005;194(39–41):4135–95.
[42] Phung-Van P, Tran LV, Ferreira AJM, Nguyen-Xuan H, Abdel-Wahab M. Nonlinear transient isogeometric analysis of smart piezoelectric functionally graded material plates based on generalized shear deformation theory under thermo-electro-mechanical loads. Nonlinear Dyn 2017;87:879–94.
[43] Phung-Van P, De Lorenzis L, Thai CH, Abdel-Wahab M, Nguyen-Xuan H. Analysis of laminated composite plates integrated with piezoelectric sensors and actuators using higher-order shear deformation theory and isogeometric finite elements. Comput Mater Sci 2015;96:495–505.
[44] Chitour M, Bouhadra A, Bourada F, Mamen B, Bousahla AA, Tounsi A, et al. Stability analysis of imperfect FG sandwich plates containing metallic foam cores under various boundary conditions. Structures: Elsevier; 2024.
[45] Hasim KA, Kefal A. A novel isogeometric layerwise element for piezoelectric analysis of laminated plates with straight/curvilinear fibers. Comput Methods Appl Mech Eng 2022;399:115440.
[46] Nguyen LB, Thai CH, Duong-Nguyen N, Nguyen-Xuan H. A size-dependent isogeometric approach for vibration analysis of FG piezoelectric porous microplates using modified strain gradient theory. Eng Comput 2022;38(5): 4415–35.
[47] Phung-Van P, Hung PT, Tangaramvong S, Nguyen-Xuan H, Thai CH. A novel Chebyshev-based both meshfree method and shear deformation theory for functionally graded triply periodic minimal surface flat plates. Comput Struct 2025;309:107660.
[48] Thai CH, Hung PT, Rabczuk T, Nguyen-Xuan H, Phung-Van P. A Chebyshev shear deformation model for laminated composite plates. Compos Struct 2025;360: 119045.
[49] Yang W, Liang X, Shen S. Electromechanical responses of piezoelectric nanoplates with flexoelectricity. Acta Mech 2015;226(9):3097–110.
[50] Xu L, Shen S. Size-dependent piezoelectricity and elasticity due to the electric field-strain gradient coupling and strain gradient elasticity. Int J Appl Mech 2013;5(02): 1350015.
[51] Hu S, Shen S. Electric field gradient theory with surface effect for nano-dielectrics. Computers, Materials & Continua (CMC) 2009;13(1):63.
[52] Shu L, Wei X, Pang T, Yao X, Wang C. Symmetry of flexoelectric coefficients in crystalline medium. J Appl Phys 2011;110(10):104106.
[53] Reddy JN. Theory and analysis of elastic plates and shells. CRC Press; 2006.